Transcriptomics and proteomics characterizing the antioxidant mechanisms of semaglutide in diabetic mice with cognitive impairment

YING YANG, LULU SONG, LIPING YU, JINPING ZHANG and BO ZHANG

Department of Endocrinology, China-Japan Friendship Hospital, Beijing 100029, P.R. China

Received October 16, 2024; Accepted January 16, 2025

DOI: 10.3892/ijmm.2025.5497

Abstract. The aim of the present study was to investigate the neuroprotective effects of semaglutide in diabetes-associated cognitive decline (DACD), while also exploring the underlying mechanisms targeting anti-oxidative effects. The present study evaluated the antioxidant properties of semaglutide using a DACD model of inflammation. To investigate the underlying mechanisms, omics technologies were employed. Comprehensive transcriptomic and proteomic analysis of the cells was conducted to identify the pathways responsible for the observed antioxidant effects. Semaglutide demonstrated the potential to enhance learning and memory functions while mitigating hippocampal pathological damage. RNA-sequencing and data-independent acquisition proteomics analyses identified 13,511 differentially expressed genes and 588 differentially expressed proteins between the control and type 2 diabetes mellitus (T2DM) groups. In addition, 1,378 genes and 2,394 proteins exhibited a differential expression between the T2DM and semaglutide (10 μg/kg) treatment groups. A combined transcriptomic and proteomic analysis unveiled 40 common pathways. Acyl-CoA oxidase 1 (ACOX1) was observed to be activated during oxidative stress and subsequently suppressed by semaglutide. Of note, the antioxidant and anti-apoptotic properties of semaglutide in high glucose (HG) conditions were partially reversed upon ACOX1 overexpression. Overall, the present data provided molecular evidence to elucidate the physiological connections between semaglutide and neuronal function, and contribute to clarifying the role of semaglutide in combating oxidative stress and HG-induced cognitive impairment.

Correspondence to: Professor Bo Zhang, Department of Endocrinology, China-Japan Friendship Hospital, 2 Yinghuayuan East Street, Hepingli, Chaoyang, Beijing 100029, P.R. China
E-mail: drbozhang@yahoo.com

Key words: diabetes, cognitive, transcriptomic, proteomic, oxidative stress

Introduction

Diabetes-associated cognitive decline (DACD) is a chronic complication of diabetes with a complex pathogenesis (1). Diabetic patients face a notably higher risk of cognitive impairment, which manifests as decreased memory, reduced cognitive flexibility and, in severe instances, intellectual decline and behavioral abnormalities. This results in a decline in patients' self-management abilities and an increased dependency on caregivers, which further accelerates the progression of diabetes, creating a vicious cycle. (2). According to a previous study (3), DACD affects ~30% of patients with diabetes. Compared with the general population, patients with DCI are more likely to develop Alzheimer's disease. This significantly increases the economic burden on families and society, emerging as a worldwide health problem that requires immediate attention and resolution.

The etiology of DACD is complex, and its pathogenesis has not been completely clarified (4). A previous study reported that insulin resistance is not only a significant feature of diabetes but is also associated with diabetic cognitive dysfunction, particularly in patients with type 2 diabetes mellitus (T2DM) (5). Chronic hyperglycemia in patients with diabetes results in neuronal damage and cognitive decline, predominantly impacting the hippocampus and prefrontal cortex-regions crucial for memory and executive function. The impact of oxidative stress on neuronal cells has been extensively studied, revealing that it can lead to various forms of cellular damage, including apoptosis and necrosis. For instance, in a study involving SH-SY5Y neuronal cells, it was demonstrated that oxidative stress resulted in increased reactive oxygen species (ROS) production, which subsequently led to decreased cell viability and enhanced necrotic cell death (6). In diabetes, oxidative stress arises from various sources, including hyperglycemia and mitochondrial dysfunction, leading to an imbalance in the redox state of neuronal cells (7). Oxidative stress underlies numerous pathologies, including neuroinflammation (8), apoptosis (9) and neurological disorders/neurodegeneration (10,11). It is clear that there is a need for the development of treatment methods that can both lower blood sugar levels and target these specific pathways. It is crucial to conduct research aimed at identifying hypoglycemic drugs with neuroprotective properties.

In recent years, there has been growing interest in discovering a new class of drugs with significant biological activities and numerous clinical benefits derived from glucagon-like peptide-1 (GLP-1) receptor agonists used in glucose-lowering therapy (12). Semaglutide is a long-acting GLP-1 analogue that shares 94% homology with human GLP-1 (13). It replicates the effects of the natural hormone GLP-1 by enhancing insulin secretion, suppressing glucagon release, and slowing gastric emptying. These actions contribute to improved blood glucose control and some benefits beyond glucose lowering (14-16). In the field of neuroscience, semaglutide has shown significant potential as a neuroprotective agent in rodent models. Its effects on seizures, neuronal damage, cognitive function and other neurobiological aspects make it a compelling candidate for further investigation in clinical settings (17). However, there are only a few studies focusing on the mechanism of semaglutide on DACD, therefore it is necessary to perform a comprehensive and systematic transcriptome and proteome analysis of DACD brain tissues.

The aim of the present study was to elucidate how semaglutide mitigates DACD and investigate the underlying mechanisms responsible for reducing oxidative stress. Integrated transcriptomic and proteomic analyses were employed to identify key factors and specific pathways associated with oxidative stress that are both activated by DACD and modulated by semaglutide.

Materials and methods

Animals. A total of 50 male C57BL/6J mice (8-week-old) were procured from Beijing SiPeiFu Biotechnology Co., Ltd. [SCXK (Jing) 2019-0004]. The mice (weight, 25-32 g) were housed in groups of four to five per cage, maintained under standard temperature conditions with a 12/12-h light/dark cycle. They had *ad libitum* access to food and water throughout the experiment. All experimental procedures and animal care protocols were approved (approval no. zryhyy61-24-02-25) by the Ethics Committee of China-Japan Friendship Hospital (Beijing, China). T2DM was induced in the mice according to a previously established protocol (18). Briefly, the mice were fed a high-fat diet (HFD) comprising 60% fat for 4 weeks. Following this, they received intraperitoneal injections of streptozotocin (STZ) at a dose of 25 mg/kg/day for 5 consecutive days. Control mice were administered an equivalent volume of PBS (1X) intraperitoneally for the same duration after a 4-week period of feeding on a standard chow diet. Diabetes was confirmed if blood glucose levels exceeded 300 mg/dl 16 days after the final STZ injection. Blood glucose levels were measured using Accu-Chek glucose strips from tail vein blood samples. After establishing the model, mice were administered subcutaneous injections of either saline or semaglutide every day for 16 weeks leading up to the behavioral experiment. Diabetic mice (n=20 per group) were randomized into two groups: The T2DM and semaglutide (Sema) groups. The mice in both groups were fed an HFD diet. Mice in the sema group received daily subcutaneous injections of semaglutide (Novo Nordisk) at a dose of 10 μg/kg. The dosing regimen for semaglutide began with 2.5 μg/kg/day during the first week, increased to 5 μg/kg/day in the second week, and then was maintained at 10 μg/kg/day for the rest of the study. The dosage of semaglutide was determined based on previous studies (19,20) and the results of the preliminary experiments. In our preliminary experiments, no adverse effects were observed in mice following this administration strategy. This gradual adjustment may help reduce gastrointestinal side effects and optimize therapeutic efficacy. Mice received an equal volume of 0.9% saline and were fed with a regular diet. Subsequently, the mice were fasted overnight (12 h) and administered their final dose of semaglutide or saline at 08:00.

Morris water maze (MWM) test. The MWM test was used to evaluate spatial learning and memory capacity. The study protocol has been previously described in detail (21). The test was conducted 16 weeks after the establishment of the model in a grey circular pool with a diameter of 150 cm, divided into four equal quadrants, each filled with water maintained at 30±2˚C and with a depth of 16 cm. An overhead camera was positioned centrally above the pool and linked to a computerized recording system equipped with a tracking program (DigBehv; Shanghai Jiliang Software Technology Co., Ltd.) capable of monitoring and recording the swimming paths of the mice.

The testing protocol involved conducting four trials on the platform each day over a 5-day acquisition phase, followed by a probe trial on day 6. During the acquisition phase, mice were placed in a water pool within a quadrant where the platform was not present, and given 60 sec to locate the hidden platform. If a mouse failed to find the platform within this time frame, it was gently guided to the platform and allowed to stay there for 15 sec, reinforcing memory of the platform's location. Data were recorded at the 90-sec mark. This procedure was repeated four times daily until performance improvements plateaued. On day 6, the platform was removed, and each mouse was allowed to swim freely for 60 sec from the same starting position, which was opposite the original platform location. The time spent in the target quadrant and the total swimming duration were recorded for further analysis.

Novel object recognition (NOR) and novel object location recognition (NOL) tests. The NOL and NOR tests were used to assess learning and memory functions in each group, following established protocols (22). These tests were administered 16 weeks after the model was established. Initially, mice were acclimated to an empty wooden chamber for 15 min. After a 24-h period, each mouse was placed back in the same chamber, where two identical objects were positioned in the corners. The mice were allowed to explore the chamber freely until they had spent a total of 30 sec interacting with both objects. Exploration was defined as the mouse approaching an object with its nose within 2 cm; climbing or sitting on the object was not considered exploration.

After another 24-h period, the mice were returned to the chamber, where one of the familiar objects was replaced with a new object located in a different corner. The preference for the novel object was measured by the proportion of time spent exploring the new object compared with the total time spent exploring both objects. A total of eight mice from each group were randomly selected for the tests. The NOL test was conducted first, followed by the NOR test 4 days later. During the NOR test, 24 h after the initial exploration phase,

one of the familiar objects was replaced with a new one, and the percentage of time spent exploring the novel object was calculated as a proportion of the total time spent exploring both objects.

Hematoxylin and eosin (H&E) staining. Brain tissues were collected following the completion of behavioral experiments. The mice were anesthetized using 70% CO_2 narcosis and subsequently euthanized via cervical dislocation. To assess the extent of the neuronal damage, the authors adhered to the H&E staining protocol provided by Beijing Solarbio Science & Technology. Histological changes in the hippocampal regions were examined using an optical microscope (Olympus Corporation) at a magnification of x200. Neuronal counts were conducted in the CA1, CA3, DG pyramidal cell layers and cortex by counting neurons per 250 μm segment across five sections per mouse, with the average count representing the final result.

TUNEL staining. The apoptosis assays were conducted using the TUNEL Apoptosis Assay kit (cat. no. C1088; Beyotime Institute of Biotechnology), according to the manufacturer's protocol. Hippocampal sections were initially fixed with 4% paraformaldehyde for 30 min at room temperature, followed by two washes with 0.01 M PBS (10 min each), and a 5-min incubation at room temperature with 0.5% Triton X-100/PBS. The TUNEL assay solution was then applied to the slides, which were covered with anti-evaporation film and incubated at 37˚C for 60 min in the dark. After staining the cellular nuclei with DAPI (5 μg/ml) for 10 min at room temperature, the slides were washed three times, each wash lasting 5 min. Finally, the slides were cover-slipped using a 50% glycerin mounting medium. The stained tissue sections were examined using a fluorescence microscope (Olympus Corporation). A total of five randomly selected fields were observed under the microscope at a magnification of x200 to determine the total number of neurons and the count of TUNEL-positive neurons. The percentage of apoptotic neurons was calculated using the formula: (TUNEL-positive neurons/total neurons) x100%.

Transcriptome analysis. For the RNA sequencing (RNA-seq) experiments, hippocampus samples were isolated and sent to Huada Gene Research Institute (Guangdong, China) for RNA preparation and sequencing. A total of three mice from each group were randomly selected to serve as biological replicates, and their total RNA was extracted using the TRIzol® reagent kit (Thermo Fisher Scientific, Inc.). The quality of the extracted RNA was assessed using the Agilent 2100 Bioanalyzer (Agilent Technologies, Inc.). Samples with A260/A280 ratios >1.8 were further evaluated. Subsequently, mRNA was enriched and fragmented into shorter sequences and reverse-transcribed into cDNA. The second-strand cDNA was synthesized using a second-strand synthesis reaction system (Invitrogen; Thermo Fisher Scientific, Inc.). The second-strand cDNA was subsequently purified, end-repaired, polyadenylated and ligated to Illumina sequencing adapters (Illumina, Inc.). The resultant products were sequenced using the Illumina HiSeq 2500 platform (Illumina, Inc.).

Principal component analysis (PCA) and Pearson correlation coefficient (PCC) were performed with the R package gmodels (23). The clean data were aligned to the Mus musculus genome (GRCm38). Next, the data were aligned to the reference gene sequence using Bowtie 2 (http://bowtie-bio.sourceforge.net/bowtie2/index.shtml), and the expression levels of genes and transcripts were calculated using RNA-Seq by Expectation-Maximization. Differential expression analysis was conducted using DESeq2 (https://github.com/mikelove/DESeq2). Genes with a P<0.001 (adjusted using the Benjamini and Hochberg method) and a fold change of >2.0 were identified as differentially expressed. These differentially expressed genes (DEGs) were classified and enriched using Gene Ontology (GO) and Kyoto Encyclopedia of Genes and Genomes (KEGG) pathway annotation.

Quantitative proteomics analysis. A total of three replicates of each group of hippocampus samples were measured in parallel. The proteomic analysis was conducted at the Jingjie PTM BioLab Co., Ltd. Proteomics Facility, following established protocols (24). Proteins extracted from hippocampal cell lysates were quantified using bicinchoninic acid assay. The proteins were subjected to trypsin digestion at a protein-to-protease ratio of 50:1 (w/w) for 12 h. Next, protein was subjected to cysteine reduction and alkylation using sequential incubation with 5 mM dithiothreitol at 56˚C for 30 min and 11 nM iodoacetamide for 15 min at room temperature in the dark. The resulting peptides were resuspended in mobile phase A (0.1% formic acid +2% acetonitrile) for subsequent liquid chromatography, and were separated using a NanoElute ultrahigh-performance liquid chromatography system (Bruker Daltonics; Bruker Corporation). The gradient for phase B (0.1% formic acid +100% acetonitrile) was programmed as follows: 6-24% from 0-70 min, 24-35% from 70-84 min, 35-80% from 84-87 min and 80% from 87-90 min, with a flow rate of 450 nl/min. During the separation process, peptides were ionized using a capillary ion source and subsequently analyzed using a TIMS-TOF Pro mass spectrometer (Bruker Daltonics). The pulse voltage was set at 1.65 kV, and peptide precursors along with their secondary fragments were analyzed using high-resolution LC/Q-TOF-MS. The scan range for the secondary mass spectrometry was set between 400 and 1,500 m/z.

The DESeq2 R software package (version 3.14) was used to conduct differential expression analysis among the three groups. Fold-changes were calculated to compare the three groups. Proteins with an adjusted P<0.05 and an absolute fold-change >1.2 were considered differentially expressed. The GO and KEGG pathway enrichment analyses of differentially expressed proteins (DEPs) were conducted using clusterProfiler (version 3.4.4, https://guangchuangyu.github.io/software/clusterProfiler). Gene Set Enrichment Analysis (GSEA) was performed using GSEA software (version 4.1.0, http://www.broadinstitute.org/gsea).

mRNA and protein correlation analyses. First, DEGs and DEPs were identified among the groups. Genes with a fold change ≥1.2 and P<0.05 were considered significant DEGs, while proteins with a fold change of >1.5 and P<0.05 were considered significant DEPs. Subsequently, the association between genes and proteins was quantitatively analyzed. The detected genes/proteins and the DEGs/DEPs in both the transcriptome and proteome were counted separately. A Venn

diagram was created using this data. In addition, a nine-quadrant map analysis was performed to illustrate the correlation between genes and proteins. This analysis was conducted using R language (version 3.5.1). To assess functional enrichment, GO biological process (BP) terms and KEGG pathway analysis of mRNAs were applied to the nine-quadrant map. A correlation analysis between GO functions and KEGG pathway information in the transcriptome and proteome was carried out, comparing the similarities and differences in gene function and metabolic pathways between the two groups.

Western blot analysis. Total proteins were extracted by the Total Protein Extraction Kit (cat. no. KGB5303; Nanjing KeyGen Biotech Co., Ltd.). The protein concentrations were determined by the bicinchoninic acid assay. Following the quantification of the total protein concentration extracted from primary microglia *in vitro*, a loading buffer was added to the samples for high-temperature denaturation. Denatured protein samples (20 μg) were then separated using SDS-PAGE (Wako Supersep™ Ace, 5-20%) and transferred onto PVDF membranes (Invitrogen; Thermo Fisher Scientific, Inc.) soaked in transfer buffer. To prevent non-specific binding, the membranes were blocked with 5% non-fat milk for 1 h at room temperature. Primary antibodies against Acyl-CoA oxidase 1 (ACOX1; 1:5,000; cat. no. PA5-76341; RRID: AB_2720068), GLP-1R (1:2,000; cat. no. PA5-97790; RRID: AB_2812405) and β-actin (1:5,000; cat. no. MA1-140; RRID: AB_2536844; all from Invitrogen; Thermo Fisher Scientific, Inc.) were applied at 4˚C to the blots overnight. After washing with Tris-buffered saline containing 0.05% Tween-20 (TBST), the protein bands were incubated with an anti-rabbit IgG HRP-linked secondary antibody (1:3,000; cat. no. CST-7074S; Cell Signaling Technology, Inc.) at room temperature for 1 h. The fluorescence intensity of the specific antibody on the protein bands was then detected using an enhanced chemiluminescent reagent (Bio-Rad Laboratories, Inc.). The resulting blots were quantified via densitometric analysis using ImageJ (Image Lab 4.1; Bio-Rad Laboratories, Inc.). Uncropped blots are shown in Fig. S1A-E.

Reverse transcription-quantitative polymerase chain reaction (RT-qPCR). Tissue and cell lysis were conducted using a TRIzol-based cell lysis buffer (Invitrogen; Thermo Fisher Scientific, Inc.). Following this, complementary DNA (cDNA) synthesis was performed with the PrimeScript™ RT reagent kit (cat. no. RR037A; Takara Bio, Inc.), following the manufacturer's protocol. The PCR cycle parameters were as follows: 94˚C for 2 min; 40 cycles with denaturation at 94˚C for 20 sec, annealing at 60˚C for 20 sec and extension at 72˚C for 20 sec. Gene expression levels were then quantified through qPCR analysis using SYBR-Green mix (Roche Diagnostics). The primer sequences used are provided in Table SI. β-actin was used as the reference gene for normalizing mRNA expression levels. Analysis of relative gene expression data was conducted using the $2^{-\Delta\Delta Cq}$ method (25).

Cell culture. Primary hippocampal neuronal cultures were generated from C57BL/6 mice using standard protocols (26). Primary hippocampal neurons were isolated from P0-P1 wild-type mouse pups. Hippocampi were dissected, dissociated with 0.25% trypsin, and plated onto poly-D-lysine-coated coverslips (for imaging) or 6-well plates (for biochemical analysis) at a density of 7,500 cells/cm. Hippocampal neuronal cultures were cultured in neurobasal medium supplemented with GlutaMax (Gibco; Thermo Fisher Scientific, Inc.) and B-27 and incubated at 37˚C with 5% CO_2 in a humidified incubator. To simulate an *in vivo* model of diabetes induced by HFD and STZ, an *in vitro* approach using high glucose (HG) supplemented with palmitic acid (Pal) was employed as previously described (26). The HG+Pal medium contained 200 μM Pal and 25 mM glucose.

Administration of plasmids, small interfering (siRNA) or semaglutide. GLP-1 receptor (GLP-1R) expression in primary hippocampal neurons was silenced using siRNA transfection. Primary hippocampal neurons were transfected with GLP-1R siRNA (50 nM; Shanghai GeneChem Co., Ltd.) using Lipofectamine® 2000 (Thermo Fisher Scientific, Inc.) at 37˚C, according to the manufacturer's protocol. The inhibitory efficiency was verified using western blotting (Fig. S2A). A total of 6 h post-transfection, the medium was replaced with one containing 5% FBS for 24 h before proceeding with additional experiments. In order to investigate whether semaglutide could regulate oxidative stress through ACOX1, ACOX1 overexpression was accomplished via pcDNA3.1-ACOX1-GFP transfection. Primary hippocampal neurons were divided into the following groups: i) Control group (NC); ii) HG + Pal group; iii) HG + Pal + Sema group (HG + Pal + Sema); iv) HG + Pal + siRNA GLP-1R group (HG + Pal + siRNA GLP-1R); v) HG + Pal + siRNA NC group; vi) HG + Pal + Sema + pcDNA3.1-ACOX1-GFP group; and vii) HG + Pal + Sema + pcDNA3.1-GFP group. pcDNA3.1-ACOX1-GFP and pcDNA3.1-GFP were purchased from Thermo Fisher Scientific, Inc. Cells were cultured with or without semaglutide (4 μg/ml, 99.84%, HY-114118; MedChemExpress) and incubated for 48 h at 37˚C. Following treatment, cells were prepared for immunofluorescence, western blotting, and oxidative and antioxidant measurements.

Examination for H_2O_2, catalase (CAT), malondialdehyde (MDA), superoxide dismutase (SOD) and glutathione (GSH). Hippocampal supernatants and primary hippocampal cultures were assayed for mouse oxidative stress levels (CAT, MDA, SOD and GSH) using testing kits from Nanjing Jiancheng Bioengineering Institute (cat. nos. A007-2-1, A003-1-2, A001-1-1 and A006-1-1, respectively). H_2O_2 levels were tested using a commercial kit (cat. no. S0038; Beyotime Institute of Biotechnology). All procedures were conducted according to the manufacturer's protocol.

Cell viability. The viability of primary hippocampal cultures following exposure to pcDNA3.1-ACOX1-GFP or pcDNA3.1-GFP was assessed using a Cell Counting Kit-8 assay (cat. no. CK04; Dojindo Molecular Technologies, Inc.) at the time points of 0, 12, 24 and 48 h. Briefly, cells were seeded into 96-well plates at a density of 2,000 cells per well and cultured until confluence. Next, 10 μl of CCK-8 solution was added to each well and incubated at 37˚C for 2-3 h. Optical absorbance at 450 nm was then measured using a microplate reader (Tecan Group, Ltd.).

Adeno-associated virus administration. To increase ACOX1 expression in mice, AAV8-Alb-ACOX1 or AAV8-Alb-eGFP which was resuspended in PBS was injected into the tail vein at a dose of 1e11 gc per mouse. Hippocampal tissues were collected 16 weeks after semaglutide treatment and 3 weeks post-AAV injection. The activation efficacies are shown in Fig. S2B.

Immunofluorescence. For immunofluorescence, the 4-μm sections were first deparaffinized with xylene and rehydrated with an ethanol series. Next, they were blocked with goat serum for 1 h and then incubated overnight at 4˚C with primary antibodies against NEUN (1:500; cat. no. PA5-78499; RRID: AB_2736206), 4HNE (1:50; cat. no. MA5-27570; RRID: AB_2735095; both from Invitrogen; Thermo Fisher Scientific, Inc.), followed by incubation with secondary antibodies conjugated with Alexa Fluor 488 (green) and Alexa Fluor 594 (red) (1:500; cat. no. A-11001; RRID: AB_2534069; 1:500; cat. no. A-11012; RRID: AB_2534079; Invitrogen; Thermo Fisher Scientific, Inc.) for 2h at room temperature. After mounting on slides, the samples were examined and imaged using a Zeiss Axio Observer 3 fluorescence microscope (Carl Zeiss AG). ImageJ software (v. 1.53; National Institutes of Health) was used to measure the mean fluorescence intensity, and 4HNE-positive and NEUN-positive cells were manually counted.

Statistical analysis. Statistical analysis was performed using one-way ANOVA with Tukey's or Dunnett's post-hoc tests for multiple comparisons, utilizing GraphPad Prism 7 software (GraphPad Prism Software, Inc.; Dotmatics) unless otherwise noted. Quantitative data from three independent biological replicates are presented as the mean ± standard deviation. Unless otherwise specified, all experiments were conducted with three independent biological replicates. A two-sided $P<0.05$ was considered to indicate a statistically significant difference.

Results

Hyperglycemia has the potential to impair cognitive function. A flow chart for the experiments is shown in Fig. 1A. In the NOL test, control mice spent more time exploring the object placed at a new location (Fig. 1B). Mice in the Sema group spent significantly more time attending the object in the novel location. By contrast, T2DM mice did not display any preference for either object. In both the NOL and NOR test, semaglutide improved long-term cognitive impairment in T2DM mice (Fig. 1C). Spatial learning and memory were assessed using the MWM. Mice with T2DM displayed a significantly longer time to find the hidden platform in the MWM task compared with age-matched control mice (Fig. 1D and E). Semaglutide improved the learning ability shown by decreased escape latency during the positioning navigation experiment. In subsequent probe trials, T2DM mice exhibited a decreased preference for the trained target zone compared with the NC (Fig. 1F). However, the mice in the Sema group spent significantly more time in the target quadrant than those in the T2DM group. It is noteworthy that all groups of mice swam at comparable speeds (Fig. 1G).

Hyperglycemia leads to hippocampal tissue damage. H&E staining was employed in the present study to evaluate neuronal morphology and abundance. In the control mice, hippocampal cells exhibited well-organized structures with no abnormalities in morphology (Fig. 2A). Conversely, hyperglycemia in mice with T2DM resulted in neuronal damage and loss within the hippocampus and cortex compared with controls. Microscopic analysis revealed disrupted cellular patterns and pyknotic nuclei in T2DM mice. Semaglutide treatment could ameliorate cell morphology changes and cytoplasmic contraction in HG conditions, with these alterations being particularly prominent in the hippocampus. Of note, hippocampal dysfunction is considered the primary pathological foundation for cognitive decline observed in individuals with T2DM.

TUNEL staining was performed to evaluate neural cell apoptosis. The hippocampus of T2DM mice exhibited a significantly higher number of TUNEL-positive cells compared with the controls (Fig. 2B). There was a particularly robust decrease in apoptosis in hippocampus of semaglutide-treated T2DM mice. These results suggested that hyperglycemia may contribute to hippocampal damage and promote neural cell death through apoptosis (Fig. 2C).

Transcriptomics analysis. To identify changes in gene expression, RNA-seq analysis was performed to examine the transcriptome in mice from three groups. PCA of the results revealed significant differences in transcripts between the control and T2DM groups (Fig. S3A). Box plots showing distribution of log10-transformed intensity of identified RNAs in three groups (Fig. S3B) suggested that the quality of the RNA samples was favorable. The Pearson correlation coefficient (PCC) showed a high correlation between biological replicates, while it was low when comparing the (-) dimethyl sulfate (DMS) and (+) DMS libraries for each biological replicate (Fig. S3C).

Following this analysis, bar charts (Fig. 3A) and volcano plots (Fig. 3B and C) were used to visualize the DEGs induced by the various treatments. RNA-seq identified 74,693 genes when comparing the NC to the T2DM group, and the T2DM group to the Sema group, respectively. Within the Control vs. T2DM comparison, 13,511 genes were differentially expressed, with 8,472 upregulated and 5,039 downregulated (Fig. 3B). Compared with the T2DM group, Sema treatment resulted in 1,378 DEGs, including 740 upregulated and 638 downregulated genes (Fig. 3C). Next, the DEGs in the three groups are shown using heatmaps (Fig. 3D and E). The top 10 DEGs significantly upregulated/downregulated in these three groups are listed in Table I. These plots revealed a distinct separation in the transcriptional profiles between the three groups, with biological replicates clustering tightly together. This observation suggested that T2DM and semaglutide treatment resulted in differential gene expression patterns.

Molecular alterations in proteomics. During our proteomic analysis, a comprehensive quality evaluation was performed to ensure the accuracy of the results. This involved assessing sample repeatability through analysis of peptide length distribution, peptide quantity distribution, PCC, PCA and the relative standard deviation tests (Fig. S3D-F). The distribution of the protein intensity profile and peptide length distribution

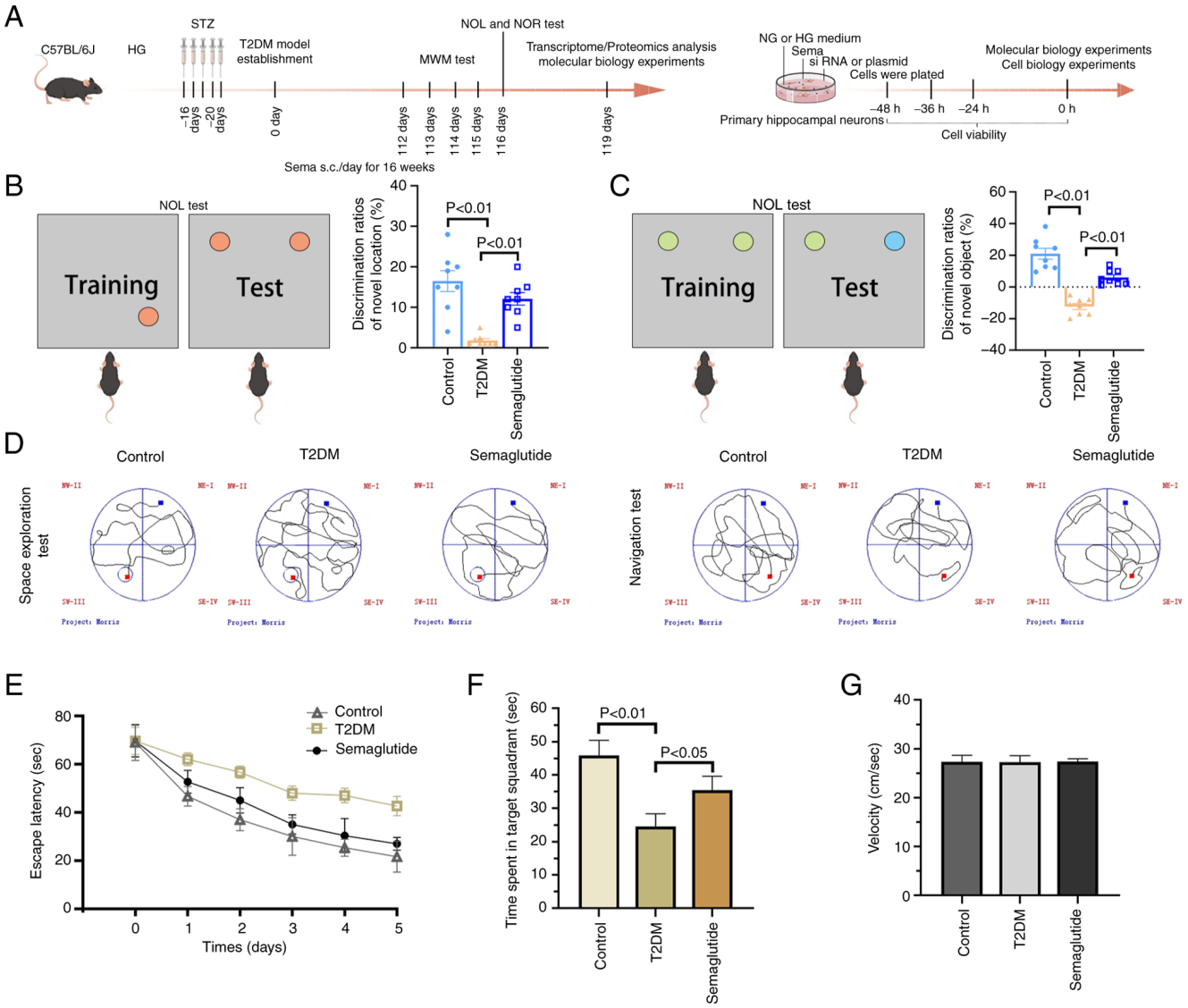

Figure 1. Hyperglycemia has the potential to impair cognitive function. (A) Experimental design. (B) Schematic drawing of novel location and quantification of the ratio of exploration time on novel objective location in both groups of mice. (C) Schematic drawing of novel objective object and quantification of the ratio of exploration time on novel objective object in both groups of mice. (D) Path map of the MWM. (E) Average escape latency from the positioning navigation tests. (F) Time spent in target quadrant in space exploration tests. (G) Swim speed during MWM trials. Data are presented as the mean ± SD (n=3). MWM, Morris water maze; T2DM, type II diabetes mellitus; NOR, novel object recognition; NOL novel object location recognition.

of the identified peptides are revealed in Fig. S3G and H. The hippocampi of the T2DM group demonstrated significant changes in protein expression compared with the NC. In total, 588 proteins were DEPs, with 413 being upregulated and 175 downregulated (Fig. 4A and B). Similarly, the Sema group exhibited 2,394 DEPs in the hippocampus when compared with the T2DM group. Similar to the T2DM group, these DEPs consisted of 718 upregulated and 1,676 downregulated proteins (Fig. 4A and C). Heatmaps (Fig. 4D) and radar plots (Fig. 4E and F) visually represent the protein expression patterns between the Control vs. T2DM and T2DM vs. Sema groups. The top 10 DEPs significantly upregulated/downregulated in these three groups are listed in Table II.

Common trends of DEPs and DEGs. The present analysis revealed an interesting trend. When comparing T2DM and NC groups across different pathways, a higher number of upregulated genes was identified, compared with downregulated genes. In addition, the Sema group displayed a decrease in more genes compared with the T2DM group (Fig. 5A and B). This pattern mirrored what was observed at the protein level. These findings suggested the potential existence of common genes significantly altered by hyperglycemia and subsequently restored by semaglutide treatment. The list of the DEPs reversed by semaglutide between T2DM/Control and Sema/T2DM is shown in Table SII. The list of the top 200 DEGs reversed by semaglutide between T2DM/Control and Sema/T2DM is presented in Table SIII.

GO and KEGG pathway enrichment analysis. To uncover the key BPs involved in semaglutide's improvement of DACD, GO enrichment results were examined from the comparisons between the Control and T2DM groups, as well as between the T2DM and Sema groups. The results revealed a significant enrichment of DEGs and DEPs in pathways associated with cell survival, transport and catabolism,

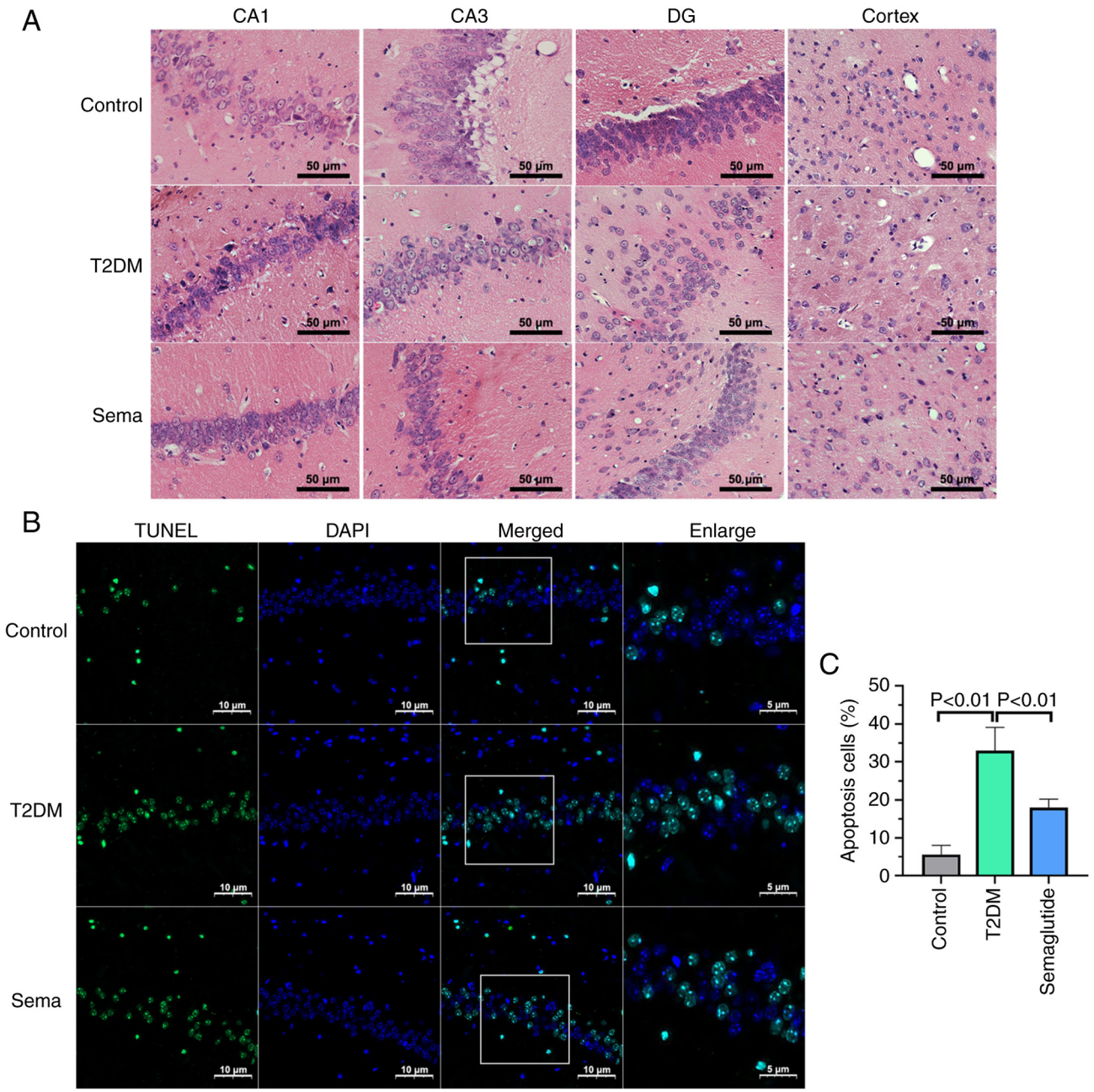

Figure 2. Hyperglycemia leads to damage in hippocampal tissue. (A) Representative images of H&E staining in CA1, CA3, DG and Cortex zones (magnification, x400). (B) Representative confocal images depict neuronal apoptosis in hippocampal tissues, indicated by TUNEL (green) and DAPI (blue) staining. (C) The bar graph illustrates the relative percentage of apoptotic neuronal cells in the hippocampal tissue, determined through TUNEL staining, across the three groups of mice (n=3). Data are presented as the mean ± SD. Graphs are representative of three independent experiments. T2DM, type II diabetes mellitus.

as well as signal transduction (Fig. 5C and D). DEGs and DEPs exhibited significant GO enrichment with respect to 20 GO-BP, 44 GO-cellular component and 26 GO-molecular function terms (Table SIV). To identify key pathways underlying semaglutide's improvement in hyperglycemia-induced cognitive decline, KEGG pathway enrichment results from Control vs. T2DM and T2DM vs. Sema comparisons were analyzed using R software (R software, version 3.2) (Fig. 5E and F). This identified 40 commonly enriched pathways (Table SV). Fatty acid degradation was observed, along with metabolic pathways, fatty acid metabolism and cAMP signaling pathways due to the enrichment in both the Control vs. T2DM and T2DM vs. Semaglutide comparisons (Table SVI). This combined analysis revealed commonly enriched ACOX1 in these pathways.

The correlation between transcriptome and proteome. An integrated analysis was conducted to investigate the correlation between mRNA and protein levels. Genes in the Control and T2DM groups that showed both increased mRNA and protein levels (defined as a log2 fold change >0.263034) were selected. A total of 86 genes (54 upregulated and 32 downregulated) exhibited significant changes in both mRNA and protein levels in the DM compared with the NC group (Fig. 6A). In addition, 155 genes (26 upregulated and 129 downregulated) displayed differentially expressed mRNA and protein levels in the

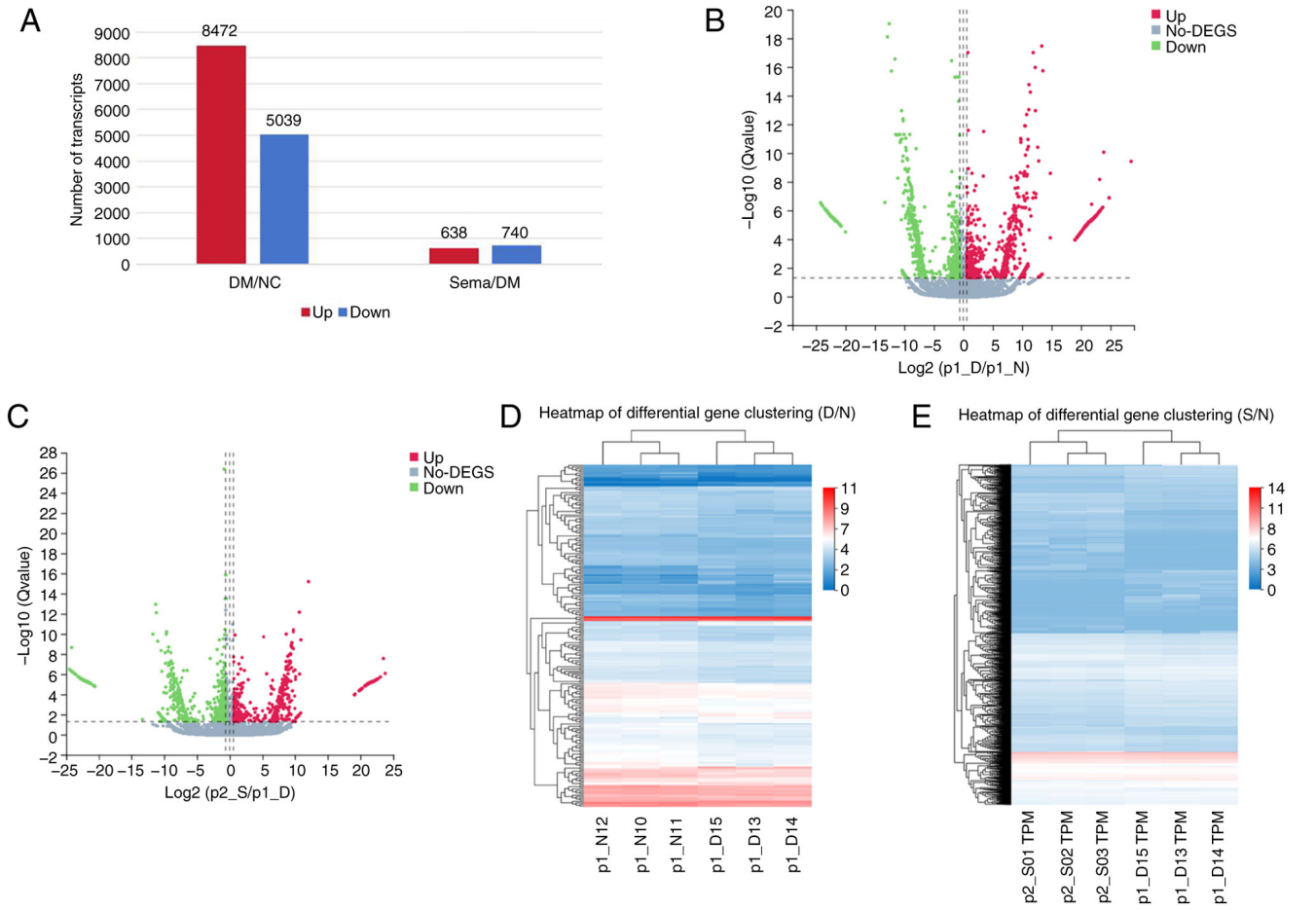

Figure 3. Differential analysis in RNA expression levels in the hippocampus of different groups. (A) Histogram of differential gene expression among different groups. (B and C) Volcano plots showing relative abundances of transcripts in three groups. The transcripts were considered differentially expressed at fold change >1.5 and with statistical significance (P<0.05) between groups. The green points represent the downregulated genes, and the red points represent the regulated genes that were statistically significant. (D and E) Heatmaps of selected DEGs in different groups, where light red represents high expression and light blue represents low expression. DEGs, differentially expressed genes.

Sema group relative to the DM group (Fig. 6B). Among them, ACOX1 exhibited a significantly altered expression in the DM group compared with the NC group, but was downregulated in the Sema-treated group compared with the T2DM group.

Antioxidant effects of semaglutide inhibited by ACOX1. Analysis of the transcriptome and proteome revealed a correlation between ACOX1 and protective effects of semaglutide on the hippocampus of mice with T2DM. This warrants further investigation. In T2DM mice, ACOX1 expression in the hippocampus was significantly higher compared with the NC group (Fig. 6C). Conversely, hippocampal tissues in the Sema group showed a significant reduction in ACOX1 induction compared with the DM mice. This trend was consistent with ACOX1 transcription levels (Fig. 6D). As illustrated in Fig. 6E and F, the high-glucose challenge significantly increased oxidative stress markers, including H_2O_2 and MDA, in the hippocampus of T2DM mice, which were reduced by Sema treatment. Meanwhile, antioxidants such as CAT, SOD and GSH were significantly restored in the hippocampus of Sema-treated T2DM mice (Fig. 6G-I). AAV8-Alb-Acox1 was then used to increase ACOX1 expression and assess the oxidant and antioxidant capacities. Even with Sema present, AAV8-Alb-Acox1 treatment consistently elevated oxidative stress levels and reduced antioxidant defense enzymes (Fig. 6J-N). Immunofluorescent staining confirmed that the hippocampal lipid peroxidation product 4-HNE was significantly induced by T2DM, but greatly reduced in mice supplemented with Sema (Fig. 6O). Furthermore, compared with the DM + Sema group, mice co-treated with Sema and AAV8-Alb-Acox1 revealed a higher fluorescent intensity of 4-HNE (Fig. 6P), indicating increased oxidative stress.

A cell viability assay demonstrated that exposure to pcDNA3.1-GFP did not affect cell viability. There was no observable change in cell viability over time in the pcDNA3.1-GFP-treated group. pcDNA3.1-ACOX1-GFP did not produce a significant loss of cell viability until 48 h post exposure (Fig. 7A). pcDNA3.1-ACOX1-GFP overexpression efficacy was analyzed using western blotting and PCR (Fig. S2C). In primary hippocampal neuron cultures, HG + Pal treatment led to an increase in ACOX1 expression, whereas GLP-1R agonism resulted in its decrease. Following GLP-1R inhibition, ACOX1 protein expression was significantly elevated. The transcriptional expression results were consistent with the protein results (Fig. 7B and C). The level of oxidative stress, including that of H_2O_2, MDA, CAT, SOD and GSH, was then assessed. As expected from the results, HG + Pal treatment significantly upregulated H_2O_2 and MDA,

Table I. List of top 10 differentially expressed genes significantly upregulated/downregulated in these three groups.

	T2DM/Control		
Gene ID	Gene symbol	Type	Log2(FC)
100038882	Isg15	mRNA	1.602249511
100042074	Gm3650	mRNA	4.32462459
118568284	LOC118568284	mRNA	-1.40967923
12642	Ch25h	mRNA	-2.389526237
20344	Selp	mRNA	-4.309909401
226040	Tmem252	mRNA	-1.754036809
231290	Slc10a4	mRNA	1.514550901
238393	Serpina3f	mRNA	-4.175723916
442834	D830031N03Rik	mRNA	-1.520722637
54123	Irf7	mRNA	2.166235551
	Sema/T2DM		
Gene ID	Gene symbol	Type	Log2(FC)
107303348	Gm45935	mRNA	6.151632936
108167670	Gm17415	mRNA	-6.377687627
108168832	Gm13981	mRNA	-6.312064864
110312	Pmch	mRNA	6.728818468
118567798	LOC118567798	mRNA	-7.511450723
15171	Hcrt	mRNA	7.901759599
216036	Gm4796	mRNA	-7.158297767
353204	Aldoart1	mRNA	-9.75033781
433319	Gm5528	mRNA	-6.96612261
433745	Gm12816	mRNA	-7.234313084

T2DM, type 2 diabetes mellitus.

downregulating CAT, SOD and GSH. This was effectively reversed by semaglutide treatment (Fig. 7D-H). Hippocampal neurons treated with siRNA GLP-1R showed increased oxidative stress levels, indicating that GLP-1R negatively regulates ACOX1 expression. In addition, neurons co-treated with Sema and pcDNA3.1-ACOX1-GFP exhibited higher levels of H_2O_2 and MDA compared with those treated with Sema alone. The immunofluorescence results corroborated that conclusion (Fig. 7I and J). Cells in the HG + Pal group exhibited increased immunoreactive fluorescence intensity for 4HNE compared with the NC group. However, in the HG + Pal + Sema group, the 4HNE fluorescence signal decreased in primary hippocampal neurons. By contrast, with the presence of pcDNA3.1-ACOX1-GFP, the 4HNE fluorescence signals remained strong even after Sema treatment.

TUNEL assays revealed an increase in the number of apoptotic TUNEL-positive cells upon HG + Pal treatment, whereas semaglutide administration resulted in a decrease in these cells. The antiapoptotic effects of semaglutide in the HG + Pal treatment group were partially abolished following ACOX1 overexpression (Fig. 7L and K). These findings suggested that the neuroprotective effects of semaglutide were significantly diminished by pcDNA3.1-ACOX1-GFP treatment.

Discussion

Cognitive decline is a frequent and associated condition with diabetes (28-30). Individuals with diabetes are 1.5-2.0-fold more likely to experience cognitive decline, impairment or dementia compared with those without diabetes (31). The clinical progression of DACD typically involves three stages: Diabetes-associated cognitive decrements, mild cognitive impairment and dementia (32). While multiple potential mechanisms for DACD have been proposed (33-35), the exact cause remains unclear. Numerous attempts have been made in the treatment DACD to use agents that simultaneously lower blood glucose levels and provide neuroprotective actions. Semaglutide is a GLP-1 receptor agonist primarily used for the treatment of T2DM and obesity. Beyond its metabolic effects, recent studies have indicated that semaglutide may exert neuroprotective properties through oxidative stress reduction, anti-inflammatory effects, and promoting neuronal survival (17,20,36). The present study revealed that hyperglycemia induced impairments of learning and memory. Long-term hyperglycemia caused hippocampus damage and upregulated apoptotic cells, but these defects were reversible by semaglutide. Further systematic experiments are required

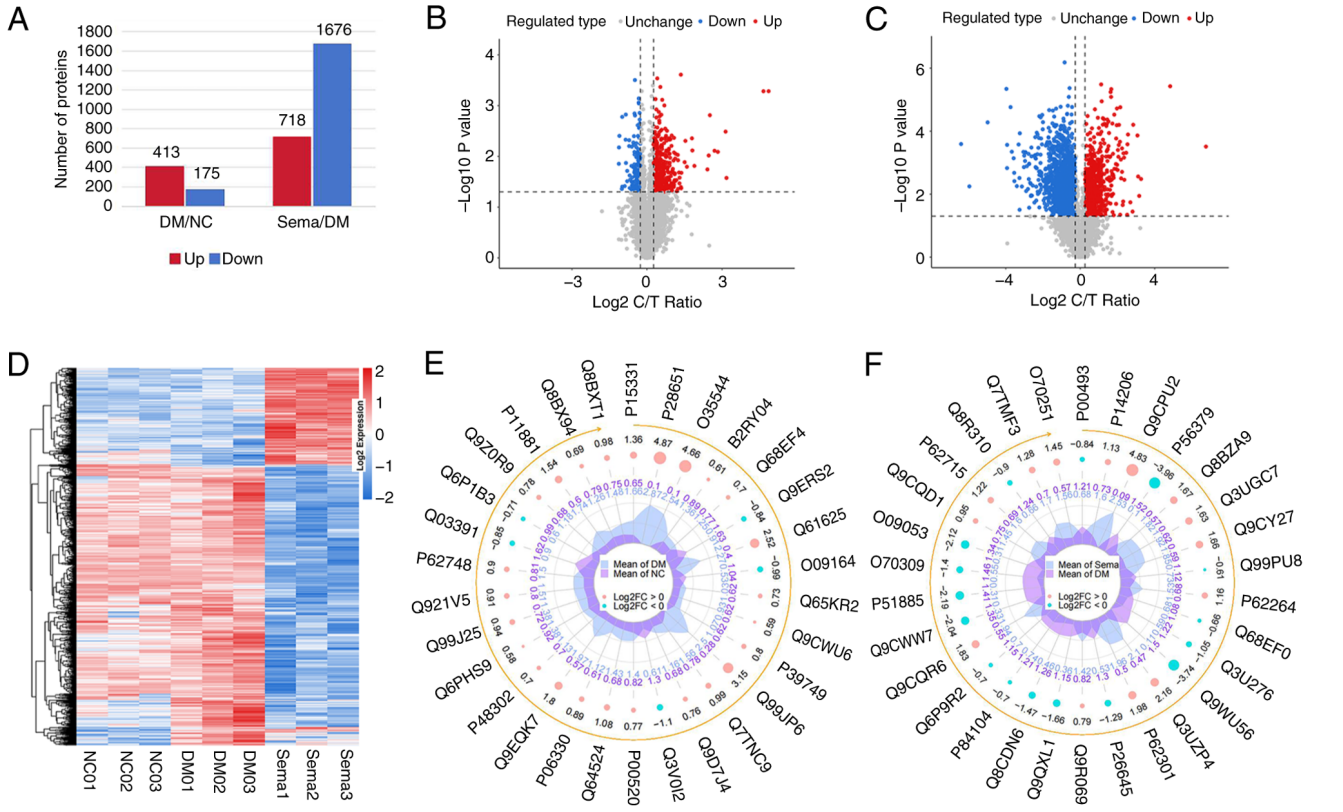

Figure 4. Differential analysis in protein expression levels in different groups. (A) Histogram of differential protein expression among different groups. (B and C) Volcano plots showing relative abundances of proteins in three groups. The proteins were considered differentially expressed at fold change >1.2 and with statistical significance (P<0.05) between groups. The red points represent the upregulated proteins, and the green points represent the downregulated proteins that were statistically significant. (D) Heatmaps of selected differentially expressed proteins in different groups, where light red represents high expression and light blue represents low expression. (E and F) Radar plots of protein expression among the different groups. DM, diabetes mellitus; NC, negative control.

to elucidate the precise mechanisms through which the specific genes and proteins identified in this study function.

High-throughput molecular biological techniques, including transcriptomics and proteomics, have been employed to investigate biological processes and the mechanisms of action of natural drugs within the realm of systems biology. An increasing number of studies indicates that the combined application of transcriptomics and proteomics presents a promising avenue for elucidating the complex molecular mechanisms underlying novel hypoglycemic agents (37,38). In the present study, a screening was performed to determine the DEGs and DEPs after inducing T2DM and administering semaglutide. It was found that the 13,511 genes and 588 proteins that were significantly upregulated in the model group were notably improved by semaglutide treatment, while 1,378 genes and 2,394 proteins significantly downregulated in the model group were also significantly ameliorated by semaglutide treatment. Upon KEGG pathway enrichment analysis of these overlapping DEGs and DEPs, 40 pathways affected by semaglutide post-T2DM were identified. These pathways primarily relate to fatty acid degradation, synaptic function and neurodegeneration. Of note, the antioxidative stress action of semaglutide was implicated in multiple factors, including ACOX1.

In previous studies, semaglutide has never been reported to reduce oxidative stress through regulating ACOX1. The metabolic enzyme ACOX1, a key rate-limiting enzyme in fatty acid β-oxidation, is expressed across various tissues (39,40). During the β-oxidation of long-chain fatty acids, ACOX1 produces H_2O_2 as a byproduct. An excessive buildup of H_2O_2 can result in oxidative stress within cells (41). Further research has shown that in the context of diabetes, especially T2DM, ACOX1 expression is significantly altered, leading to metabolic dysregulation and related complications. Previous studies using the ACOX1 knockout mouse model revealed that ob/ob mice lacking ACOX1 exhibited sustained activation of peroxisome proliferator-activated receptors in the liver, resistance to obesity, and improved glucose tolerance and insulin sensitivity (42,43). In the present study, it was shown that HG increased ACOX1 expression and oxidative stress in hippocampal tissue from T2DM mice, as well as primary hippocampal neurons treated with HG + Pal. In the context of oxidative stress, ACOX1's role becomes crucial. Loss-of-function mutations in ACOX1 have been associated with glial and axonal degeneration, underscoring its vital role in neuronal health and development (44). Furthermore, the production of H_2O_2 and ROS during mutations in ACOX1 have been associated with glial and axonal degeneration, underscoring its vital role in neuronal health and oxidative metabolism, making it particularly susceptible to oxidative stress (45). In neurons, oxidative stress not only leads to cell death but also affects neurotransmission and synaptic plasticity, thereby impairing cognitive function (46). In addition, the antiapoptotic actions of GLP-1 have been demonstrated in neuronal cell lineages. The activation of GLP-1 receptors can inhibit the apoptosis

Table II. List of top 10 differentially expressed proteins significantly upregulated/downregulated in these three groups.

T2DM/Control			
Accession	Protein name	Gene name	FC
P28651	Carbonic anhydrase-related protein	Ca8	30.73104346
Q99JP6	Homer protein homolog 3	Homer3	8.605505985
Q0VEJ0	Centrosomal protein of 76 kDa	Cep76	6.493296981
O35544	Excitatory amino acid transporter 4	Slc1a6	5.854075769
Q61625	Glutamate receptor ionotropic, delta-2	Grid2	5.678624242
Q0QWG9	Delphilin OS=Mus musculus	Grid2ip	4.508011439
Q3TGF2	Protein FAM107B	Fam107b	4.364816483
Q64338	Dual specificity calcium/calmodulin-dependent 3',5'-cyclic nucleotide phosphodiesterase 1C	Pde1c	4.229122142
Q9EQK7	Protein-S-isoprenylcysteine O-methyltransferase	Icmt	3.77526444
Q63ZW7	InaD-like protein	Patj	3.691659478
Sema/T2DM			
Accession	Protein name	Gene name	FC
Q9Z0N2	Eukaryotic translation initiation factor 2 subunit 3, Y-linked	Eif2s3y	107.9458757
Q9CPU2	NADH dehydrogenase [ubiquinone] 1 beta subcomplex subunit 2, mitochondrial	Ndufb2	28.50007876
P04104	Keratin, type II cytoskeletal 1	Krt1	9.647625063
P02535	Keratin, type I cytoskeletal 10	Krt10	9.021370593
Q3UV17	Keratin, type II cytoskeletal 2 oral	Krt76	8.672844569
P02463	Collagen alpha-1(IV) chain	Col4a1	8.439254018
A2AWR3	Lysosomal cholesterol signaling protein	Gpr155	7.209646232
O70451	Monocarboxylate transporter 2	Slc16a7	7.039011181
Q8BQP9	Regulator of G-protein signaling 7-binding protein	Rgs7bp	6.480696147
P03930	ATP synthase protein 8	Mtatp8	5.936756791

T2DM, type 2 diabetes mellitus.

of nerve cells caused by various reasons. This is primarily due to their ability to activate various intracellular signaling cascades that promote neuroprotection and cell survival (47). GLP-1 helps in the biogenesis of mitochondria and improves their overall function, resulting in increased ATP production. It can also boost energy production by enhancing glucose metabolism. By promoting insulin signaling pathways, GLP-1 helps cells to respond more effectively to insulin. In addition, GLP-1 has been shown to inhibit the activation of caspases, which are enzymes involved in the process of apoptosis (48). Furthermore, it is well known that semaglutide not only effectively lowers blood glucose levels but also regulates lipid metabolism, enhancing the function and metabolic activity of adipocytes (49). By improving fat metabolism, semaglutide may help reduce the risk of obesity-related metabolic diseases. Research has also found that semaglutide can regulate energy balance by stimulating insulin secretion, further promoting fat utilization and reducing fat storage. It was therefore hypothesized that semaglutide might regulate ACOX1 to influence the balance between oxidative stress and the antioxidant defense system, further promoting fat utilization and reducing fat storage.

Other GLP-1 receptor agonists, such as Liraglutide, have also been reported to offer multiple benefits to patients with diabetes. Long-acting and short-acting GLP-1RAs have similar mechanisms of action but different durations of drug action. Liraglutide has garnered attention for its neuroprotective properties, particularly in the context of oxidative stress associated with diabetes. Studies have demonstrated that liraglutide can effectively mitigate oxidative stress in neuronal cells, which is crucial given the

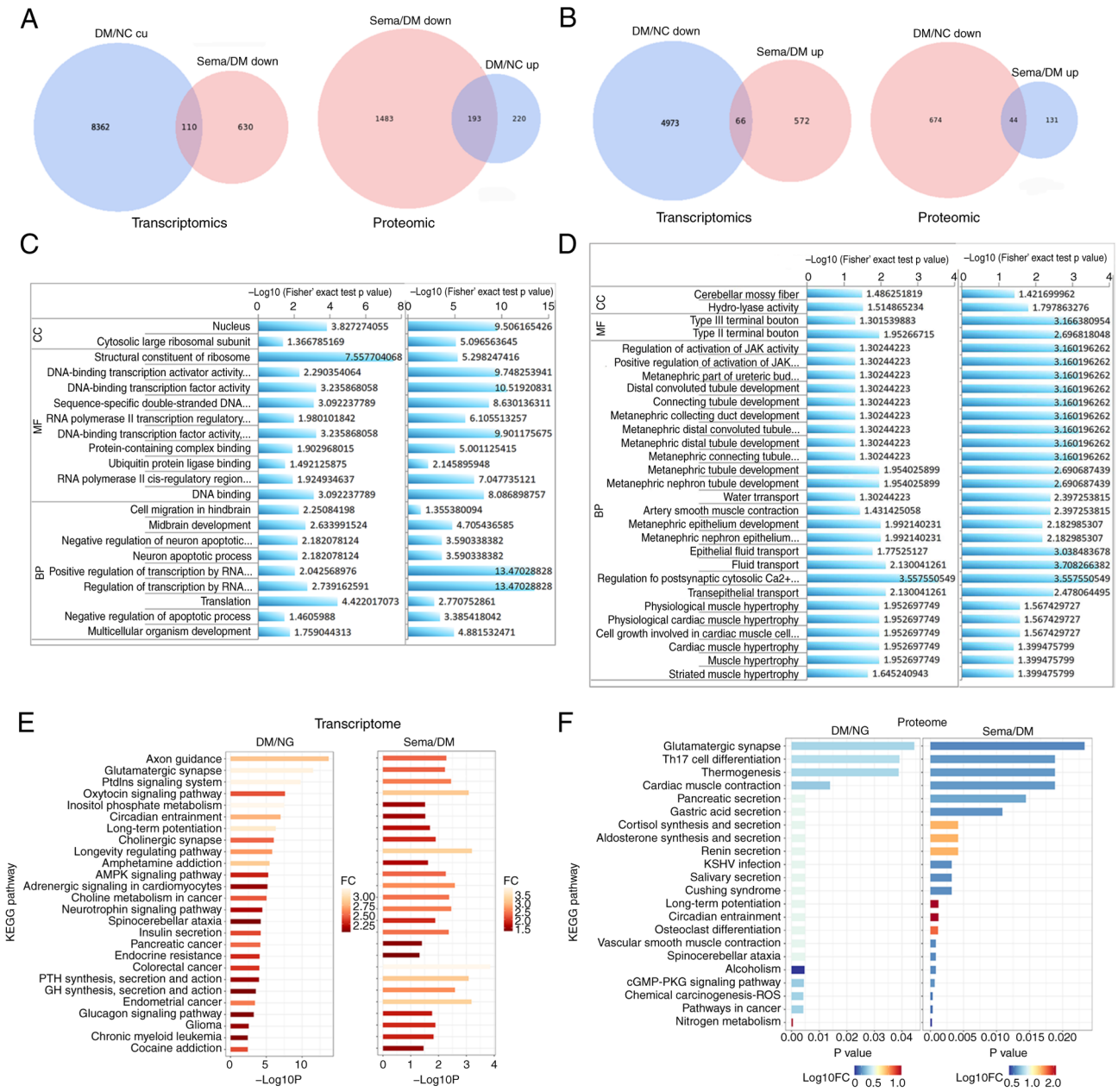

Figure 5. Common differentially expressed genes/differentially expressed proteins, GO enrichment and KEGG pathway analysis in Transcriptome and Proteome. (A) Overlapped mRNAs (left) and proteins (right) between the upregulated Control-vs.-T2DM group and decreased Sema vs. T2DM group. (B) Overlapped mRNAs (left) and proteins (right) between the decreased Control-vs.-T2DM group and upregulated Sema vs. T2DM group. (C) Overlapped GO in the Control group vs. the T2DM group (left) and Sema vs. T2DM group (right) at the transcriptomic level. (D) Overlapped GO in the Control-vs.-T2DM group (left) and Sema vs. T2DM group (right) at the proteomic level. (E) Overlapped KEGG pathways in the Control-vs.-T2DM group (left) and Sema vs. T2DM group (right) at the transcriptomic level. (F) Overlapped KEGG pathways in the Control-vs.-T2DM group (left) and Sema vs. T2DM group (right) at the proteomic level. GO, Gene Ontology; KEGG, Kyoto Encyclopedia of Genes and Genomes; T2DM, type 2 diabetes mellitus.

link between diabetes and neurodegenerative diseases such as Alzheimer's disease. For instance, liraglutide has been shown to prevent beta-amyloid-induced neurotoxicity in SH-SY5Y cells through a phosphoinositide 3-kinase (PI3K)-dependent signaling pathway, thereby inhibiting neuronal apoptosis and oxidative stress (50). This protective mechanism is particularly relevant as oxidative stress is a significant contributor to neuronal damage in diabetic conditions. Research also indicates that semaglutide can mitigate oxidative stress in neuronal cells by promoting antioxidant defenses. For instance, HFD-induced obese mice had reduced body weight, improved oxidative stress indexes, significantly increased the percentage of water maze trips and the number of platform crossings, and significantly shortened the water maze platform latency after semaglutide intervention (51). Besides diabetic animal models, semaglutide amended encephalomyelitis-induced cognitive and motor deficits, hippocampal damage and corpus callosum demyelination caused by encephalomyelitis. Additionally, semaglutide activates the PI3K/Akt axis, which eventually hampers GSK-3β activity, which boosts Nrf2 and SOD levels, inhibiting oxidative stress (52). Future comprehensive research could offer valuable insights into comparing the neuroprotective properties of these two GLP-1 receptor agonists, providing a robust theoretical foundation for their evaluation.

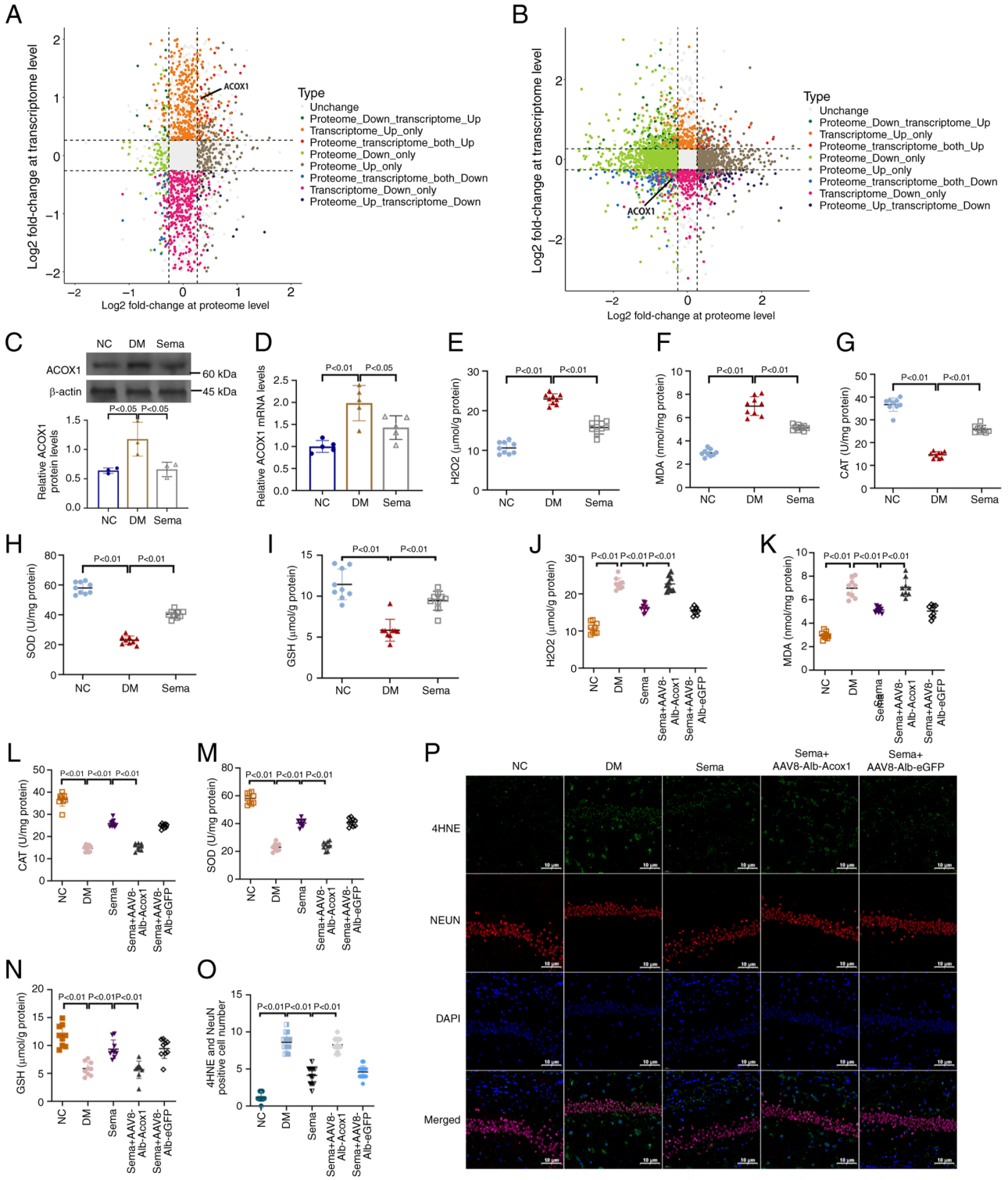

Figure 6. Correlation between transcriptome and proteome. (A) DM vs. NC. (B) Sema vs. DM, nine-quadrant graph (considering the statistical significance, P<0.05). The x-axis (abscissa) shows the log2 fold change of the protein levels. The y-axis (ordinate) shows the log2 fold change of the transcriptome levels. The top of the figure displays the Pearson correlation coefficient and its associated statistical significance (P-value) between the transcriptome and proteome data. Each dot represents a gene and its corresponding protein. Grey dots indicate genes and proteins that show no significant change in expression. Red dots represent genes and proteins that exhibit similar trends (upregulation). Blue dots represent genes and proteins that exhibit opposite trends in expression (downregulation). (C) Western blot images. (D) Quantification of western blot bands. Examination for (E) H_2O_2, (F) MDA, (G) CAT, (H) SOD and (I) GSH in hippocampus tissues of three groups of mice. Examination for (J) H_2O_2, (K) MDA, (L) CAT, (M) SOD and (N) GSH in hippocampus tissues of mice treated with or without Sema + AAV8-Alb-Acox1. n=3 (O) Immunofluorescent staining for 4-HNE expression in hippocampal sections. (P) Positive fluorescent intensity of 4-HNE was quantified after IF analysis. DM, diabetes mellitus; NC, negative control; MDA, malondialdehyde; CAT, catalase; SOD, superoxide dismutase; GSH, glutathione.

There are several limitations to the present study. First, this study reported the mechanism in regulation of antioxidative genes and proteins by semaglutide. It is possible that semaglutide enhances cognitive function by simultaneously influencing

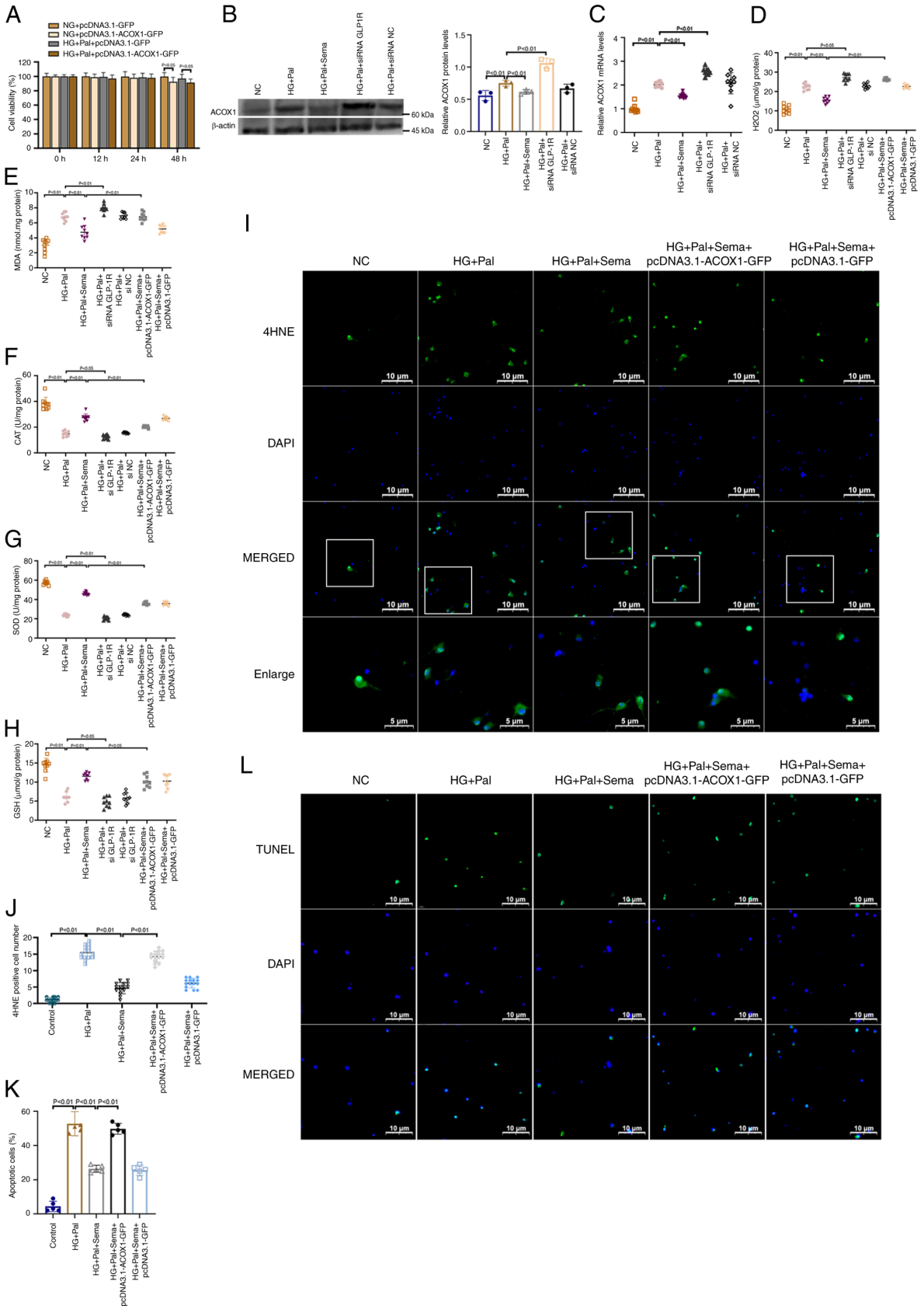

Figure 7. Semaglutide mitigates oxidative stress through the inhibition of the ACOX1. (A) The Cell Counting Kit-8 assay of cell viability of different time of pcDNA3.1-ACOX1-GFP on primary microglia (n=3). (B) Western blot analysis of ACOX1 in primary hippocampal neurons; graphs are representative of three independent experiments (n=3). (C) mRNA expression for ACOX1 in primary microglia (n=3). Examination for (D) H_2O_2, (E) MDA, (F) CAT, (G) SOD and (H) GSH in cells in all groups. (I) The representative images of immunofluorescence staining with 4HNE immunofluorescence (green) and nuclei (blue) in hippocampal neurons (magnification, x500). A total of five fields were randomly selected for observation. (J) Quantitation of immunofluorescence for 4HNE in primary neurons (n=3). (K) Bar graph of the proportion of apoptotic cells. (L) Representative confocal images show TUNEL (green) and DAPI (blue) staining of Primary microglia (magnification, x400). A total of five fields were randomly selected for observation. ACOX1, Acyl-CoA oxidase 1; MDA, malondialdehyde; CAT, catalase; SOD, superoxide dismutase; GSH, glutathione; HG, high glucose; Pal, palmitic acid; NC, negative control.

multiple biological pathways and processes rather than relying on a single mechanism. However, identifying the primary contributors to this improvement has been challenging. Further research is necessary to fully understand the various ways in which semaglutide protects the brain. Furthermore, one potential limitation of our research lies in the inherent differences between rodent and human brain structures. Consequently, further experimental evidence is necessary to substantiate the clinical applicability of the current findings.

In conclusion, the present study clarified the role of semaglutide in the hippocampus and its ability to alleviate cognitive impairments. These findings provided a scientific basis for the clinical application of semaglutide and encouraged further exploration of the potential benefits of novel glucose-lowering medications. The present study is significant as it offers a deeper understanding of how semaglutide functions to reduce oxidative stress caused by hyperglycemia.

Acknowledgements

Not applicable.

Funding

The present study was supported by National High Level Hospital Clinical Research Funding (grant nos. 2023-NHL HCRF-YXHZ-ZR-01 and 2022-NHLHCRF-YS-01) and the National Key Research and Development Program of China (grant no. 2018YFC1313902).

Availability of data and materials

The data generated in the present study may be found in the Sequence Read Archive under accession number PRJNA1176207 or at the following URL: https://dataview.ncbi.nlm.nih.gov/object/PRJNA1176207; and in the iProX under accession number PXD056999 or at the following URL: https://www.iprox.cn/page/subproject.html?id=IPX0010017001. The data generated in the present study may be requested from the corresponding author.

Authors' contributions

YY and BZ conceived the study and contributed to the interpretation of the results, accessed and verified the underlying data. YY conducted statistical analyses and drafted the first manuscript. LS, LY and JZ analyzed and interpreted the data, reviewed and revised the manuscript, and contributed in language editing. BZ provided general supervision and obtained funding. YY and BZ confirm the authenticity of all the raw data. All authors read and approved the final version of the manuscript.

Ethics approval and consent to participate

The present study was approved (approval no. zryhyy61-24-02-25) by the Ethics Committee of China-Japan Friendship Hospital (Beijing, China).

Patient consent for publication

Not applicable.

Competing interests

The authors declare that they have no competing interests.

References

1. Biessels GJ and Whitmer RA: Cognitive dysfunction in diabetes: How to implement emerging guidelines. Diabetologia 63: 3-9, 2020.
2. Biessels GJ and Despa F: Cognitive decline and dementia in diabetes mellitus: Mechanisms and clinical implications. Nat Rev Endocrinol 14: 591-604, 2018.
3. Moore EM, Mander AG, Ames D, Kotowicz MA, Carne RP, Brodaty H, Woodward M, Boundy K, Ellis KA, Bush AI, *et al*: Increased risk of cognitive impairment in patients with diabetes is associated with metformin. Diabetes Care 36: 2981-2987, 2013.
4. Simó R, Ciudin A, Simó-Servat O and Hernández C: Cognitive impairment and dementia: A new emerging complication of type 2 diabetes-The diabetologist's perspective. Acta Diabetol 54: 417-424, 2017.
5. Zilliox LA, Chadrasekaran K, Kwan JY and Russell JW: Diabetes and cognitive impairment. Curr Diab Rep 16: 87, 2016.
6. Shao J, Yang X, Liu T, Zhang T, Xie QR and Xia W: Autophagy induction by SIRT6 is involved in oxidative stress-induced neuronal damage. Protein Cell 7: 281-290, 2016.
7. An Y, Xu BT, Wan SR, Ma XM, Long Y, Xu Y and Jiang ZZ: The role of oxidative stress in diabetes mellitus-induced vascular endothelial dysfunction. Cardiovasc Diabetol 22: 237, 2023.
8. Mi Y, Qi G, Vitali F, Shang Y, Raikes AC, Wang T, Jin Y, Brinton RD, Gu H and Yin F: Loss of fatty acid degradation by astrocytic mitochondria triggers neuroinflammation and neurodegeneration. Nat Metab 5: 445-465, 2023.
9. Bridge G, Rashid S and Martin SA: DNA mismatch repair and oxidative DNA damage: Implications for cancer biology and treatment. Cancers 6: 1597-1614, 2014.
10. Zhang W, Xiao D, Mao Q and Xia H: Role of neuroinflammation in neurodegeneration development. Signal Transduct Target Ther 8: 267, 2023.
11. Cai D: Neuroinflammation and neurodegeneration in overnutrition-induced disease. Trends Endocrinal Metab 24: 40-47, 2013.
12. Drucker DJ: Mechanisms of action and therapeutic application of glucagon-like peptide-1. Cell Metab 27: 740-756, 2018.
13. Andersen A, Knop FK and Vilsbøll T: A pharmacological and clinical overview of oral semaglutide for the treatment of type 2 diabetes. Drugs 81: 1003-1030, 2021.
14. Chao AM, Tronieri JS, Amaro A and Wadden TA: Semaglutide for the treatment of obesity. Trends Cardiovasc Med 33: 159-166, 2023.
15. Marso SP, Bain SC, Consoli A, Eliaschewitz FG, Jódar E, Leiter LA, Lingvay I, Rosenstock J, Seufert J, Mark L, *et al*: Semaglutide and cardiovascular outcomes in patients with type 2 diabetes. New Engl J Med 375: 1834-1844, 2016.
16. Carney EF: A pre-specified analysis of the SELECT trial suggests a kidney benefit of semaglutide in patients without diabetes. Nat Rev Nephrol 20: 493, 2024.
17. Tipa RO, Balan DG, Georgescu MT, Ignat LA, Vacaroiu IA, Georgescu DE, Raducu L, Mihai DA, Chiperi LV and Balcangiu-Stroescu AE: A systematic review of semaglutide's influence on cognitive function in preclinical animal models and cell-line studies. Int J Mol Sci 25: 4972, 2024.
18. Zhou TT, Quan LL, Chen LP, Du T, Sun KX, Zhang JC, Yu L, Li Y, Wan P, Chen LL, *et al*: SP6616 as a new Kv2.1 channel inhibitor efficiently promotes β-cell survival involving both PKC/Erk1/2 and CaM/PI3K/Akt signaling pathways. Cell Death Dis 7: e2216, 2016.
19. McLean BA, Wong CK, Kaur KD, Seeley RJ and Drucker DJ: Differential importance of endothelial and hematopoietic cell GLP-1Rs for cardiometabolic versus hepatic actions of semaglutide. JCI Insight 6: e153732, 2021.
20. Wang ZJ, Li XR, Chai SF, Li WR, Li S, Hou M, Li JL, Ye YC, Cai HY, Hölscher C and Wu MN: Semaglutide ameliorates cognition and glucose metabolism dysfunction in the 3xTg mouse model of Alzheimer's disease via the GLP-1R/SIRT1/GLUT4 pathway. Neuropharmacology 240: 109716, 2023.
21. Vorhees CV and Williams MT: Morris water maze: Procedures for assessing spatial and related forms of learning and memory. Nat Protoc 1: 848-858, 2006.

22. Zhang B, Wang L, Zhan A, Wang M, Tian L, Guo W and Pan Y: Long-term exposure to a hypomagnetic field attenuates adult hippocampal neurogenesis and cognition. Nat Commun 12: 1174, 2021.
23. Warnes GR, Bolker B, Lumley T and Johnson RC: gmodels: Various R Programming Tools for Model Fitting. R package version 2.18.1 edition. SAIC-Frederick, Inc., New Jersey, NJ, 2018.
24. Zhang N, Jiang N, Zhang K, Zheng L, Zhang D, Sang X, Feng Y, Chen R, Yang N, Wang X, *et al*: Landscapes of protein post-translational modifications of African trypanosoma parasites. iScience 23: 101074, 2020.
25. Livak KJ and Schmittgen TD: Analysis of relative gene expression data using real-time quantitative PCR and the 2(-Delta Delta C(T)) method. Methods 25: 402-408, 2001.
26. Beaudoin GM III, Lee SH, Singh D, Yuan Y, Ng YG, Reichardt LF and Arikkath J: Culturing pyramidal neurons from the early postnatal mouse hippocampus and cortex. Nat Protoc 7: 1741-1754, 2012.
27. Nakashima H, Hamamura K, Houjou T, Taguchi R, Yamamoto N, Mitsudo K, Tohnai I, Ueda M, Urano T, Furukawa K and Furukawa K: Overexpression of caveolin-1 in a human melanoma cell line results in dispersion of ganglioside GD3 from lipid rafts and alteration of leading edges, leading to attenuation of malignant properties. Cancer Sci 98: 512-520, 2007.
28. Srikanth V, Sinclair AJ, Hill-Briggs F, Moran C and Biessels GJ: Type 2 diabetes and cognitive dysfunction-towards effective management of both comorbidities. Lancet Diabetes Endocrinol 8: 535-545, 2020.
29. Vagelatos NT and Eslick GD: Type 2 diabetes as a risk factor for Alzheimer's disease: The confounders, interactions, and neuropathology associated with this relationship. Epidemiol Rev 35: 152-160, 2013.
30. Zhang J, Chen C, Hua S, Liao H, Wang M, Xiong Y and Cao F: An updated meta-analysis of cohort studies: Diabetes and risk of Alzheimer's disease. Diabetes Res Clin Pract 124: 41-47, 2017.
31. Ennis GE, Saelzler U, Umpierrez GE and Moffat SD: Prediabetes and working memory in older adults. Brain Neurosci Adv 4: 2398212820961725, 2020.
32. Koekkoek PS, Kappelle LJ, van den Berg E, Rutten GE and Biessels GJ: Cognitive function in patients with diabetes mellitus: Guidance for daily care. Lancet Neurol 14: 329-340, 2015.
33. Arnold SE, Arvanitakis Z, Macauley-Rambach SL, Koenig AM, Wang HY, Ahima RS, Craft S, Gandy S, Buettner C, Stoeckel LE, *et al*: Brain insulin resistance in type 2 diabetes and Alzheimer disease: Concepts and conundrums. Nat Rev Neurol 214: 168-181, 2018.
34. Liu Z, Dai X, Zhang H, Shi R, Hui Y, Jin X, Zhang W, Wang L, Wang Q, Wang D, *et al*: Gut microbiota mediates intermittent-fasting alleviation of diabetes-induced cognitive impairment. Nat Commun 11: 855, 2020.
35. Marseglia A, Fratiglioni L, Kalpouzos G, Wang R, Bäckman L and Xu W: Prediabetes and diabetes accelerate cognitive decline and predict microvascular lesions: A population-based cohort study. Alzheimers Dement 15: 25-33, 2019.
36. Maskery MP, Holscher C, Jones SP, Price CI, Strain WD, Watkins CL, Werring DJ and Emsley HC: Glucagon-like peptide-1 receptor agonists as neuroprotective agents for ischemic stroke: A systematic scoping review. J Cereb Blood Flow Metab 41: 14-30, 2021.
37. Billing AM, Kim YC, Gullaksen S, Schrage B, Raabe J, Hutzfeldt A, Demir F, Kovalenko E, Lassé M, Dugourd A, *et al*: Metabolic communication by SGLT2 inhibition. Circulation 149: 860-884, 2024.
38. Sachs S, Niu L, Geyer P, Jall S, Kleinert M, Feuchtinger A, Stemmer K, Brielmeier M, Finan B, DiMarchi RD, *et al*: Plasma proteome profiles treatment efficacy of incretin dual agonism in diet-induced obese female and male mice. Diabetes Obes Metab 23: 195-207, 2021.
39. Hashimoto T: Peroxisomal beta-oxidation: Enzymology and molecular biology. Ann NY Acad Sci 804: 86-98, 1996.
40. Van Veldhoven PP, Vanhove G, Assselberghs S, Eyssen HJ and Mannaerts GP: Substrate specificities of rat liver peroxisomal acyl-CoA oxidases: Palmitoyl-CoA oxidase (inducible acyl-CoA oxidase), pristanoyl-CoA oxidase (non-inducible acyl-CoA oxidase), and trihydroxycoprostanoyl-CoA oxidase. J Biol Chem 267: 20065-20074, 1992.
41. Reddy JK and Mannaerts GP: Peroxisomal lipid metabolism. Annu Rev Nutr 14: 343-370, 1994.
42. Huang J, Jia Y, Fu T, Viswakarma N, Bai L, Rao MS, Zhu Y, Borensztajn J and Reddy JK: Sustained activation of PPAR by endogenous ligands increases hepatic fatty acid oxidation and prevents obesity in ob/ob mice. FASEB J 26: 628-638, 2012.
43. Huang J, Viswakarma N, Yu S, Jia Y, Bai L, Vluggens A, Cherkaoui-Malki M, Khan M, Singh I, Yang G, *et al*: Progressive endoplasmic reticulum stress contributes to hepatocarcinogenesis in fatty acyl-CoA oxidase 1-deficient mice. Am J Pathol 179: 703-713, 2011.
44. Chung HL, Wangler MF, Marcogliese PC, Jo J, Ravenscroft TA, Zuo Z, Duraine L, Sadeghzadeh S, Li-Kroeger D, Schmidt RE, *et al*: Loss-or gain-of-function mutations in ACOX1 cause axonal loss via different mechanisms. Neuron 106: 589-606.e6, 2020.
45. Cobley JN, Fiorello ML and Bailey DM: 13 reasons why the brain is susceptible to oxidative stress. Redox Biol 15: 490-503, 2018.
46. Cenini G, Lloret A and Cascella R: Oxidative stress in neurodegenerative diseases: From a mitochondrial point of view. Oxid Med Cell Longev 2019: 2105607, 2019.
47. Brubaker PL and Drucker DJ: Minireview: Glucagon-like peptides regulate cell proliferation and apoptosis in the pancreas, gut, and central nervous system. Endocrinology 145: 2653-2659, 2004.
48. During MJ, Cao L, Zuzga DS, Francis JS, Fitzsimons HL, Jiao X, Bland RJ, Klugmann M, Banks WA, Drucker DJ and Haile CN: Glucagon-like peptide-1 receptor is involved in learning and neuroprotection. Nat Med 9: 1173-1179, 2003.
49. Dhillon S: Semaglutide: First global approval. Drugs 78: 275-284, 2018.
50. Liu XY, Wang LX, Chen Z and Liu LB: Liraglutide prevents beta-amyloid-induced neurotoxicity in SH-SY5Y cells via a PI3K-dependent signaling pathway. Neurol Res 38: 313-319, 2016.
51. Chen X, Ma L, Gan K, Pan X and Chen S: Phosphorylated proteomics-based analysis of the effects of semaglutide on hippocampi of high-fat diet-induced-obese mice. Diabetol Metab Syndr 15: 63, 2023.
52. Sadek MA, Kandil EA, El Sayed NS, Sayed HM and Rabie MA: Semaglutide, a novel glucagon-like peptide-1 agonist, amends experimental autoimmune encephalomyelitis-induced multiple sclerosis in mice: Involvement of the PI3K/Akt/GSK-3β pathway. Int Immunopharmacol 115: 109647, 2023.